HIGH FREQUENCY PLANAR ACCELERATING STRUCTURES FOR FUTURE LINEAR COLLIDERS[1]

David Yu, Shahar Ben-Menahem
DULY Research Inc., Rancho Palos Verdes, CA 90275
Perry Wilson, Roger Miller, Ron Ruth
Stanford Linear Accelerator Center, Stanford, CA 94309
and Alireza Nassiri
Argonne National Laboratory, Argonne, IL 60439

INTRODUCTION

Modern microfabrication techniques based on deep etch x-ray lithography (LIGA)[1] can be used to produce large-aspect-ratio, metallic or dielectric, planar structures suitable for high-frequency RF acceleration of charged particle beams. Specifically, these techniques offer significant advantages over conventional manufacturing methods for future linear colliders (beyond NLC, the Next Linear Collider) because of several unique systems requirements. First, to have the required ac "wall plug" power within reasonable limits, such future linear colliders ($\geq 5 TeV$) must operate at high frequency ($\geq 30 GHz$)[2]. This implies the need of a large number of intricate accelerating structures with ever smaller dimensions and extremely tight manufacturing tolerances, imposing new challenges in mass-production, precision fabrication techniques. Microfabrication is particularly suitable for meeting this need. Secondly, luminosity requirements suggest the use of multi-bunch acceleration of electrons and positrons in the linear collider[3]. In order for these schemes to accelerate low-emittance beams over a long distance, it is important that the wakefield effects be reduced to a minimum in the accelerating structure. Asymmetric planar structures have more geometric degrees of freedom than cylindrically symmetric structures. In addition to detuning, these can be utilized to further reduce the wakefields. Thirdly, in order to clearly discriminate physics events in the final interaction point at which electrons and positrons collide, it is required that secondary particle production from beamstrahlung be minimized[4]. Flat electron and positron beams with a large aspect ratio will be beneficial in reducing beamstrahlung in the final focus region, but cause the beam to be more sensitive to wakefields in the vertical dimension. In principle, a flat beam can be accelerated in a planar structure with reduced wakefield in the vertical direction for the entire length of the accelerator.

Work is currently in progress at a number of laboratories around the world on a next-generation linear collider with a center-of-mass energy of $0.5 TeV$[5]. Designs have been proposed based on a main linac RF frequency ranging from $1.2 GHz$ (using a superconduct-ing accelerating structure - TESLA) to $30 GHz$ (a two-beam accelerator - CERN). The choice of a final design will be made late in this decade, and the machine will then be built by an international collaboration. Certainly among the strongest contenders for the final design choice is an $11.4 GHz$ main linac, based on a conventional copper accelerating structure, as proposed by SLAC and KEK. An important feature of this design is that it uses a relatively high (loaded) accelerating gradient

[1]Work supported in part by U.S. Department of Energy STTR grant no. DE-FG03-94ER86007.

(37*MV/m*), and is capable of being upgraded to 75*MV/m*. This higher gradient allows a final center-of-mass machine energy of up to 1.5*TeV* for an active linac length of about 21*km*, for an ac power of about 200*MW*[6].

The real advantage of high frequency RF becomes apparent when even higher energy linear colliders are considered. A fundamental limit on accelerating gradient is the threshold gradient for capturing an electron at rest (or with very low longitudinal velocity), to produce detrimental "dark current"[7]. While it is possible to operate at a gradient somewhat higher than this threshold gradient (61*MV/m* at 11.4*GHz*), it is dangerous to assume that a linear collider can be operated without excessive dark current at an arbitrarily higher gradient. In some SLAC NLC design options, the maximum loaded operating gradient at 11.4*GHz* is set at 75*MV/m*, or 20% above the threshold value[5].

The threshold gradient for dark current capture scales approximately as $1/\lambda$, where λ is the wavelength. Based on the NLC design, a 34*GHz* linear collider (at three times the frequency), for example, could operate at a beam-loaded gradient of 225*MV/m* (three times the gradient). This would make possible a 5*TeV* (center-of-mass energy) collider with an active linac length of about 23*km*. Although the exact frequency choice for a 5*TeV* collider is still open to question, it is clear that such a machine will require a main-linac frequency substantially higher than the NLC design frequency. Almost certainly it will be in the 25-50*GHz* range[2]. For future linear colliders with still higher center-of-mass energies, the above arguments would suggest operating at even higher frequencies. From dark current consideration only, a 25*TeV* linear collider could operate at a frequency about 90*GHz*, a low gradient on the order of 500*MV/m*, and a length about 50*km*. At such a frequency it is almost certain that the accelerating structures cannot be manufactured with conventional techniques such as machining and brazing, or even more exotic micromachining techniques[8].

The LIGA process[1] is particularly suitable for manufacturing miniaturized, planar, asymmetric cavities at high frequency. The main advantages of the LIGA process are fabrication of structures with high aspect ratio, small dimensional tolerances, and arbitrary mask shape (cross-section). Other advantages include mass-production with excellent repeatability and precision of up to an entire section of an accelerating structure consisting of a number of cells. It eliminates the need of tedious machining and brazing, for example, of individual disks and cups in conventional disk-loaded structures. Also, planar input/output couplers for the accelerating structure can be easily machined in the same process with the cavities. The new fabrication technique should substantially reduce the manufacturing cost of such accelerating structures.

PLANAR ACCELERATING STRUCTURE (PAS)

It has long been realized that flat beams have significant advantages over round beams for colliding beam machines - both circular (storage rings) and linear colliders. The advantage arises because the luminosity (L) is inversely proportional to the area of the beam cross section, while the beam-beam space charge force (F_{sc}) which causes instability in rings and beamstrahlung in linear colliders, varies roughly as the inverse of the larger transverse dimension of the beams; *i.e.*.

$$L \propto \frac{1}{\sigma_x \sigma_y} \quad ,$$

while the space charge forces are

$$F_{sc} \propto \frac{1}{\sigma_y} \quad ,$$

where σ_y and σ_x are the horizontal and vertical beam size, respectively. (Note that the vertical direction is denoted by '*x*'). Thus we want to make σ_y large while keeping the product $\sigma_x \sigma_y$ constant. Typically, future linear collider designs have σ_y about 100 times σ_x[5]. In a storage ring (either a circular collider or the damping ring for a linear collider) the vertical emittance (ϵ_x) can readily be reduced to 1/100 of the horizontal emittance by carefully decoupling the vertical motion from the horizontal. With appropriate focusing in the interaction region, it is reasonable to make the vertical amplitude function β_x also smaller than the horizontal by a factor of 100 at the collision point. The combination gives a vertical beam size at the collision point

$$\sigma_x \quad (\epsilon_x \beta_x)^{1/2} \quad \frac{\sigma_y}{100} \quad .$$

In future linear colliders it will be necessary to transport such beams with their incredibly small vertical emittances ($\gamma\epsilon_x$ =.05*mm-mr*)[5] for kilometers through high frequency (and therefore small) accelerator structures. As has been amply demonstrated at SLC, the world's (so far) only electron-positron linear collider, the most serious problem for preserving a tiny emittance is the dipole wakefields. In a conventional, circular, disk-loaded accelerating structure, the short-range dipole wakefields vary in strength approximately as $1/r^3$, where *r* is the radius of the irises. This is exactly correct for very short bunches[9].

We propose to use an asymmetric planar structure to accelerate a flat beam. In such a structure with a rectangular iris half width of *a* in the *y* direction, and *b* in *x*, the ratio of the short range horizontal wakefield force to the vertical force will vary as *b/a*. Thus, by making $b \gg a$ we can reduce the dilution of the vertical emittance due to short range wakefields in a planar structure, in which the large dimension of the beam is in the direction of the small dimension of the iris.

The SLAC future linear collider study (NLC) has a required spectrum width σ_E of the order of 10^{-3}[10]. Because the beam is tiny, a variation in acceleration with position is probably not a problem. In any case it is possible to choose cell dimensions such that the energy gain is independent of the transverse position *x* and *y*. In fact it can be proven that for a relativistic beam, if the acceleration is independent of *x*, it is also independent of *y*, and vice versa. This follows from the equation which the propagation constants satisfy:

$$k_x^2 \quad k_y^2 \quad k_z^2 \quad k^2 \quad (\frac{2\pi}{\lambda})^2 \quad .$$

The propagation constants are the constants of separation in the solutions of the wave equation using

separation of variables in rectangular coordinates. The solutions have the form:

$$E_z \quad E_o \cos(k_x x) \cos(k_y y) \cos(k_z z \quad \omega t) \quad .$$

For a relativistic beam we want $k_z = k$. Therefore:

$$k_x^2 \quad k_y^2 \quad 0 \quad .$$

Other space harmonics (for which k_z is not equal to k) enable the fields to match the boundary conditions, but do not contribute to the acceleration because they slip by $2n\pi$ in each cell. We can choose dimensions such that $k_x = k_y = 0$. This makes the acceleration independent of the transverse position for relativistic particles. Since there will be a number of large bends in future linear colliders which are much cheaper in the horizontal plane, and since bends degrade emittance, the small emittance should be in the vertical plane. It follows that the large dimension of the planar structure should be vertical for linear colliders. If we view each cell of the structure as a rectangular waveguide running vertically, $k_x = 0$ means that the waveguide as perturbed by the iris slots and by the fields from adjacent cells, appears to be at cutoff. As we have seen this automatically makes $k_y = 0$ for the velocity- of-light space harmonic.

An additional advantage of the planar accelerating structures for compact, low-energy, commercial linear accelerators as well as linear colliders, lies in the large transverse width of the beam, which can carry a high total current while maintaining a low current density, making beam transport easier in high-yield machines.

Possible planar accelerating structures, in addition to rectangular cavities described above, are muffin tins[11] and barbell cavities[12]. We will consider in this paper the simplest rectangular cells with and without a rectangular beam pipe, and will calculate the properties of these structures both analytically and numerically.

COMPARISON OF PAS WITH CIRCULAR STRUCTURE - ANALYTICAL

A planar accelerating structure can be roughly modeled as a chain of rectangular resonators, in analogy with a chain of pill box resonators for a conventional cylindrical structure. Let w be the half width, b the half height and $\alpha = w/b$ the aspect ratio of the cavity. L is the length of the cavity in the direction of beam propagation. The transit time factor T is defined as $\sin(\pi L/\lambda)/(\pi L/\lambda)$. For a rectangular resonator, the R/Q is

$$\left(\frac{R}{Q}\right)_{\square} \equiv \frac{V^2}{2\omega U} \quad 960\left(\frac{LT^2}{\lambda}\right)\frac{1}{\alpha \quad 1/\alpha} \quad .$$

Compare with the R/Q for a cylindrical pillbox resonator,

$$(\frac{R}{Q})_{\circ} \quad 483(\frac{LT^2}{\lambda}) \quad .$$

For α=1,

$$(\frac{R}{Q})_{\square} \quad 480(\frac{LT^2}{\lambda}) \qquad (\ 0.7\%)$$

For α=2,

$$(\frac{R}{Q})_{\square} \quad 0.80(\frac{R}{Q})_{\circ} \qquad (\ 20\%)$$

Q for a rectangular resonator is:

$$Q_{\square} \quad \frac{296}{R_s}[\frac{(1\ \ \alpha^2)^{3/2}}{(1\ \ \alpha^3)\ \ (\lambda/4L)(1\ \ \alpha^2)^{3/2}}] \quad .$$

where R_s is a surface resistance. Compare with a pillbox resonator,

$$Q_{\circ} \quad \frac{453}{R_s}[\frac{1}{1\ \ 0.383(\lambda/L)}] \quad .$$

For L=λ/3, or the $2\pi/3$ mode,

$$Q_{\circ} \quad \frac{211}{R_s} \quad .$$

For α=1, L=λ/3,

$$Q_{\square}(\lambda/3) \quad \frac{203}{R_s} \qquad (\ 4\%)$$

while for α=2, L=λ/3,

$$Q_{\square}(\lambda/3) \quad \frac{190}{R_s} \qquad (\ 10\%)$$

PROPERTIES OF RECTANGULAR CAVITIES WITH BEAM PIPE

We present below some MAFIA[13] calculations of the properties of a planar accelerating

structure (PAS) which consists of rectangular cells connected by a rectangular beam slit.

Fig. 1 depicts a fine-mesh, quarter-geometry of a single PAS cell. The cavity and slit dimensions shown in the figure represent what we call the `standard design'. The axial direction is denoted *z*, the height direction *y* and the (uniform) width direction is *x*. (Note that the height direction is thus horizontal). The two symmetry planes used in the quarter-geometry runs are $x=0$ and $y=0$; their intersection is the *z*-axis, which is a corner of the quarter-structure. We shall refer to the *z* axis as `the axis' below. The total length of the (repeating) cell in *z* direction, in *mm*, is denoted $L_{per}$. The uniform *x* extent is always 2*cm* (1*cm* for the 1/4 geometry shown). The half-height of the cavity is denoted `*b*' and measured in *mm*, while the half-height of the slit connecting adjacent cavities, is denoted `*h*' (also in *mm*). The *z* extent of a cavity is $L_{cav}$ (in *mm*), while the slit thickness in *z*-direction is `*t*' (*mm*). (In Fig. 1, the slit is split in two halves to create the basic repeating cell). Obviously one has: $L_{per}=L_{cav}+t$.

Frequency Domain Calculations

In frequency domain, a periodic boundary condition in the *z* direction is imposed, with phase shift φ. To ensure synchronicity for the fundamental $2\pi/3$ (accelerating) mode, φ is chosen to be 120°, and for any given *h* value, *b* is varied until the fundamental mode has the frequency $f=11.4GHz$. In accordance with the synchronicity condition, L_{per} is chosen to be $\lambda/3$, where λ is the vacuum wavelength corresponding to the above frequency. Thus $L_{per}\approx 8.775mm$.

Once such a synchronous geometry is found, a second run is performed with a slightly different φ value, in order to determine the group velocity. The *h* values we used in the frequency-domain runs were as follows (in *mm*): 0.395, 0.800, 1.00, 1.30, 2.00, 3.00, 3.70, 7.00. Of these values, the `standard design' shown in Fig.1 is $h=3.7$, corresponding to $h/\lambda=0.14$, whereas the smallest slit height has $h=0.395mm$ and $h/\lambda=0.015$. The other dimensions in Fig. 1 are: $b=9.93mm$, $L_{cav}=7.5647mm$, $t=1.2104mm$.

Numerical Results

The mesh depicted in Fig. 1 was utilized in the runs for transverse variation of synchronous voltage (Figs. 3a and 3b). For Figs. 2a through 2c, a coarser transverse mesh was used: the *x* mesh is uniform (7 divisions of the half-interval 0 to 1*cm*), while the *y* mesh has 5 uniform divisions from 0 to *h*, and another 5 uniform divisions between *h* and *b*. (The corresponding numbers for the finer mesh of Fig. 1 are 12, 10 and 5, respectively, with the *x*-mesh nonuniform and denser near the axis). Both meshes have the following *z* divisions: 16 for the full slit-thickness, 98 on either side of the cavity, and 40 uniform divisions of the cavity itself.

Fig. 2a shows the data points of cavity height (*b*) vs. slit height (*h*) at synchronicity. Fig. 2b shows the group velocity (v_g) versus *h*, where the group velocity is measured in percents of *c*, the speed of light in vacuum. The v_g values were computed by varying the boundary-condition phase from 120° to 128°, and measuring the fundamental-mode frequency shift. That this shift in phase is small enough was verified by also running at $\varphi=112^\circ$, and ascertaining linearity of the function $f(\varphi)$ in that phase range.

Fig. 2c shows the fundamental-mode axial loss factor along the axis, k_l, defined as $k_l=V^2/4U$, where V is the synchronous voltage, integrated along $x=y=0$, while U is the total stored energy (both quantities are defined per cell). The unit of k_l is V/pC.

Figs. 3a and 3b show the transverse variation of the longitudinal voltage for the 'standard geometry'. The ordinate in both figures is the synchronous voltage per cell, normalized to unity at the axis ($x=y=0$). Fig. 3a depicts the x-dependence for $y=0$, while Fig. 3b depicts the y-dependence at $x=0$. It is seen that both curves show smooth transverse variations of E_z (integrated through a cell at the speed of light): Fig. 3a fits a cosine very well, whereas Fig. 3b is well represented by a cosh curve. In particular, the curvatures of $E_{acc}(x)$ and $E_{acc}(y)$ at the axis are equal and opposite, as required by Maxwell's equations.

In the limit of vanishing slit height ($h \to 0$), the following analytical formulae apply. The loss factor is

$$k_l \quad 8Z_o c \frac{L_{cav} T^2}{\lambda^2} \frac{1}{\alpha \quad 1/\alpha}$$

where $Z_o=377\Omega$. For a synchronous $2\pi/3$ mode, $L_{cav} < L_{per} = \lambda/3$. The $h \to 0$ limit of $b(h)$ is given implicitly by the equation:

$$\left(\frac{4}{\lambda}\right)^2 \quad \frac{1}{w^2} \quad \frac{1}{b^2} \quad .$$

Upon substituting $w=10mm$, $\lambda=2.631cm$ (corresponding to a frequency of $f=11.395GHz$ which we used in our runs) and $L_{cav}=7.565mm$, we find the following theoretical values (`0' argument refers to h): $b(0)=8.73$, $k_l(0)=3.696V/pC$, which are in as good an agreement with the intercepts of Figs. 2a and 2c, respectively, as can be expected with the coarse mesh used. Points (diamonds) representing these theoretical values were added to the respective plots, with squares used to denote the numerical data points.

Time Domain Calculations

Long-range longitudinal and transverse wake potentials of the planar accelerating structure were calculated by running the T3 (time domain) module of MAFIA3[13]. The beam has a single Gaussian bunch, is stiff (no backreaction of fields on particles allowed) and assumed to have $\beta=1$. Wakefields as a function of s, the distance behind the bunch head, were measured in a postprocessor, and divided by the number of cells to yield wakefields per cell. Varying numbers of cells were used, to ensure approximate convergence to the (theoretical) case of an infinite periodic structure. This was necessary since periodicity cannot be enforced in the time-domain simulation. In addition, a pipe (extended slit) was added on either side of the multicell structure (both downstream and upstream); each was assigned an axial extent of six cavity lengths, $6L_{cav} \approx 4.5cm$, although one of the wakefields runs was also repeated with a shorter lead-in pipe. The purpose of the pipes was to ameliorate the z-direction end effects which would result from lack of periodicity.

Two different geometries were used, each with a variable number of cells. The mesh used differed between the two geometries. One geometry, which we refer to as the L-geometry, was used for a quarter-structure simulation of the longitudinal (z) wakes, and is close to the `standard design'. The other geometry is denoted T-geometry (for transverse). It corresponds exactly to the 'standard design' referred to above, and was used for half-structure simulations of the transverse (dipole-mode) wakes for off-axis beam drives. Which half of the geometry was simulated depends on the transverse drive position: for a beam driven off axis at x=0, the (magnetic) symmetry plane is x=0, whereas for a beam at y=0 and x not equal to 0, it is at y=0. We used two distinct horizontal (y) drive positions in the former case, and a single vertical (x) drive position for the latter case. In the L-geometry, the beam was driven along the axis (x=y=0).

Longitudinal and transverse wakes (per cell) were plotted at several transverse positions. In the case of transverse wakes, we have also compiled a table of rms estimate of wake amplitudes as a function of (x,y), for the three different off-axis beam drives.

The L- and T-geometries have different meshes and beam characteristics as described below.

Fig. 4 is a detailed exposition of the quarter-structure L-geometry. The dimensions are close to standard: h=3.5mm, b=9.6mm. A total of 7 cells are depicted. L_{cav} is 7.57mm. The x-mesh is uniform, at Δx=2mm (5 divisions between 0 and 1cm). The y-intervals (0,h) and (h,b) are each divided into 3 divisions. The z-mesh is uniform (this uniformity is enforced by the T3 module), with Δz=0.075mm. The beam has a single, Gaussian bunch with σ_z=0.8mm =0.03λ, and a cutoff of 3 sigmas is used on either side of the bunch center in the z-direction.

The T-geometry corresponds exactly to the 'standard design'. It has a coarser z-mesh (with Δz twice the L-geometry value) but a finer transverse mesh. The x-mesh has 7 uniform divisions in the interval from 0 to 1cm. The y-mesh has 5 uniform divisions in (0,h), and 4 divisions in the interval (h,b).

Numerical Results

We provide a plot of longitudinal wakefield (Fig. 5a). It depicts a plot of the z-wake per cell, extracted from a 14-cell run, measured at x=y=0.

The three off-axis drives which we used were at the following positions, in mm --

1) vertical position at (1.43, 0)
2) horizontal position at (0, 0.74)
3) horizontal position at (0, 1.48)

Fig. 5b shows the per-cell integrated y-wake (for a 14-cell structure), for case 3, measured at the axis (0, 0). Fig. 5c shows the per-cell x-wake (for a 14-cell structure) for the vertical drive (case 1), again measured at the axis. The same x wakefield, computed with a shorter lead-in pipe (3cm rather than 4.5cm), was found to be almost identical.

The transverse wakes (x and y) were measured throughout the transverse extent of the slit,

for the three drives. The (simulated) measurements were taken in a subgrid which subsamples the full transverse grid, by about a factor of two in either the x or y directions. Only the nonzero wakes are relevant: y-wakes for the horizontal drives, and x-wakes for the vertical drive. For the vertical drive, the relevant half-geometry is that half with non-negative y, while for the other two drives it is the non-negative x half. For the vertical drive, the measurement subgrid consisted of the (x,y) grid points

$(2i\text{-}8, 2j\text{+}1)$; i=1 to 7, j=0 to 2 (21 points in total).

For the horizontal drives, on the other hand, the subgrid has the following 20 points:

$(2i\text{+}1, 2j\text{-}10)$; i=0 to 3, j=3 to 7 .

For each of the 61 wake measurements, the variance of the per-cell wake potential was calculated, taking into account 1635 s-values at separation $\Delta s = \Delta z$, corresponding to a total s interval of 12.3cm for L-geometry, or 24.8cm for T-geometry. Finally, the *rms* wakes are extracted, and divided by the number of cells, for dipole and higher-order modes of the relevant symmetry class. Tables 1a-c list these rms wakes by drive and measurement positions.

SUMMARY

We make a comparison between a planar accelerating structure (PAS) analyzed here, and a disk-loaded, cylindrically-symmetric accelerating structure (CAS) having the same group velocity ($v_g/c \approx 0.06$). For this group velocity the CAS has $a/\lambda = 0.175$, where a is the radius of the disk opening, compared to $h/\lambda = 0.14$ for the PAS, where h is the half-height of the slit. The elastance (equal to four times the loss factor) for the accelerating mode is 600$V/pC/m$ for the PAS, or about 73% compared to the elastance (820$V/pC/m$) for a CAS with the same group velocity[14]. In the CAS the accelerating field is exactly uniform over the beam aperture for a mode which is synchronous with an electron moving close to the speed of light. For the PAS, the variation in the x direction (parallel to the slit) is given quite closely by $E_{acc}(x) \approx cos(\pi x/2w)$, where w=10mm is the half slit width (see Fig. 3a). Normal to the slit (see Fig. 3b), $E_{acc}(y) \approx cosh(\pi y/2w)$ to a good approximation. For a flat bunch oriented with the long dimension in the y direction (normal to the slit width), the field is flat to within 0.1% over a region Δx, $\Delta y = \pm 285 \mu m$. From these expressions, it is evident that the integrated, synchronous E_z satisfies the 2-D Laplace's equation in the (x,y) plane, as predicted by theory.

It is also of interest to compare the transverse wakefields. For the PAS, the wake in the x direction (normal to a flat bunch and parallel to the slit direction) is dominated by a dipole mode with a frequency of about 17.5GHz and a peak amplitude of 0.45$V/pC/$cell, when driven by a beam 1.43mm off axis. In Ref.[15], Fig. 3a, the dipole wake for a CAS driven at a=0.175λ is calculated to be 0.78$V/pC/$cell at S-band. Scaling this to 11.4GHz (multiplied by 4), the wake would be 3.1$V/pC/$cell at r_q=a=0.175λ=4.6mm and 0.97$V/pC/$cell at r_q=1.43mm. Thus the transverse lowest-frequency dipole wake in the PAS is about 45% that for a CAS with comparable group velocity. The deflection wake in the y direction does not seem to be as strongly dominated by a single dipole mode frequency (see Fig. 5b). The strongest component has a frequency of about 10GHz, and an amplitude of 0.8$V/pC/$cell. This is about 80% of the scaled CAS wake.

The deflection wakes can be compared on the basis of *rms* values. From Ref.[15], Table I, the total *rms* wake for a CAS at $r_q=a=0.175\lambda$ is about 0.55*V/pC/*cell. Scaling again to 11.4*GHz* and the 1.43*mm x* drive position, we predict a *rms* wake of 0.68*V/pC/*cell. Table 1c gives a value of 0.35*V/pC/*cell for a PAS, again lower by a factor of about 0.5. If the PAS is driven at 1.48*mm* in the *y* direction, the *rms y* wake mesured on the axis is 0.50*V/pC/*cell. This is about 90% of the wake in the scaled CAS.

ACKNOWLEDGMENT

We would like to thank Thomas Weiland for several helpful discussions on the use of MAFIA3.

REFERENCES

1. W. Ehrfeld *et al.*, "Sensor Construction Techniques via X-Ray Lithography, "Technical Digest, IEEE Solid State Sensor and Actuator Workshop, pp. 1-4, 1988; H. Guckel *et al.*, "On the Application of Deep X-Ray Lithography with Sacrificial Layers to Sensors and Actuator Construction," Transducer '91.

2. P.B. Wilson *et al.*, "Summary of RF Power Sources", Proceedings of this workshop.

3. R.D. Ruth *et al.*, "The Next Linear Collider Test Accelerator", Fifth International Workshop on Next Generation Linear Colliders (LC93), SLAC, Stanford, CA, October 13-21, 1993.

4. K. Yokoya and P. Chen, "Beam-Beam Phenomena in Linear Colliders" in Frontiers of Particles Beams, Intensity Limitations, Lecture Notes in Physics, M. Dienes *et al.*, Eds., V. 400, p. 415; R. Helm and J. Irwin, "Final Focus Systems for Linear Colliders", SLAC-PUB 5876, Proc. of Linac Conference, Ottawa, 1992, p. 258; T.O. Raubenheimer, "Preservation of Low Emittance Flat Beams", SLAC-PUB 6117, 1993.

5. See, for example, Proceedings of Fifth International Workshop on Next Generation Linear Colliders (LC93), SLAC, Stanford, CA, October 13-21, 1993.

6. P.B. Wilson, "NLC Scenarios", Table 1, SLAC NLC Note 1, August, 1994.

7. R.H. Helm and R. Miller, "Particle Dynamics" in Linear Accelerators, P.M. Lapostolle and A.L. Septier, Eds., North Holland Publishing Company, Amsterdam, 1969, p. 115.

8. J. Haimson and B. Mecklenburg, "Design and Construction of a 33 GHz Brazed Accelerating Waveguide for High Gradient Operation", Proceedings of IEEE Particle Accelerator Conference, Paper 928, 1987.

9. K. Bane and M. Sands, "Wakefields of Very Short Bunches in an Accelerating Cavity", SLAC-PUB 4441, November, 1987.

10. K.A. Thompson and R.D. Ruth, "Simulation and Compensation of Multibunch Energy

Variation in Next Linear Collider", Proceedings of the 1993 Particle Accelerator conference, p. 3693.

11. H. Henke and W. Bruns, "A Broad-Band Side Coupled mm-Wave Accelerating Structure for Electrons", Proceedings of Particle Acceletor Conference, Washington D.C., 1993, p. 904.

12. D.U.L. Yu and P.B. Wilson, "Sheet Beam Klystron RF Cavities", Proceedings of the 1993 Particle Accelerator Conference, Washington D.C., 1993, p. 2681.

13. MAFIA, Release 3.1, T. Weiland and the MAFIA Collaboration, Darmstadt, Germany, October 1991.

14. K.A. Thompson *et al.*, "Design and Simulation of Accelerating Structures for Future Linear Colliders", SLAC-PUB 6032, November, 1993.

15. D.U.L. Yu and P.B. Wilson, "Long-Range Wakefields of Disk-Loaded Structures", Particle Accelerators 30, pp.65-72 (1990). (The wake potentials in Figures 1 and 2 of this paper should be multiplied by a factor of 10.)

Table 1 *rms* estimates of transverse wakes (*V/pC/*cell) for three drive positions

x and *y* denote transverse coordinates (*mm*) in the T-geometry mesh

Table 1a drive position at (0, 0.74)
wakes measured at:

x \ *y*	-2.96	-1.48	0	1.48	2.96
0	.92	.49	.28	.49	.99
2.86	.78	.42	.21	.42	.78
5.72	.64	.28	.14	.35	.64
8.58	.28	.14	.07	.14	.35

Table 1b drive position at (0, 1.48)
wakes measured at:

x \ *y*	-2.96	-1.48	0	1.48	2.96
0	1.06	.64	.49	.71	1.13
2.86	.85	49	.35	.57	.92
5.72	.71	.42	.28	.42	.78
8.58	.35	.21	.14	.21	.42

Table 1c drive position at (1.43, 0)
wakes measured at:

x \ *y*	0	1.48	2.96
-8.58	1.63	1.70	1.84
-5.72	1.27	1.34	1.48
-2.86	.78	.78	.92
0	.35	.35	.42
2.86	.78	.78	.92
5.72	1.34	1.34	1.48
8.58	1.63	1.70	1.84

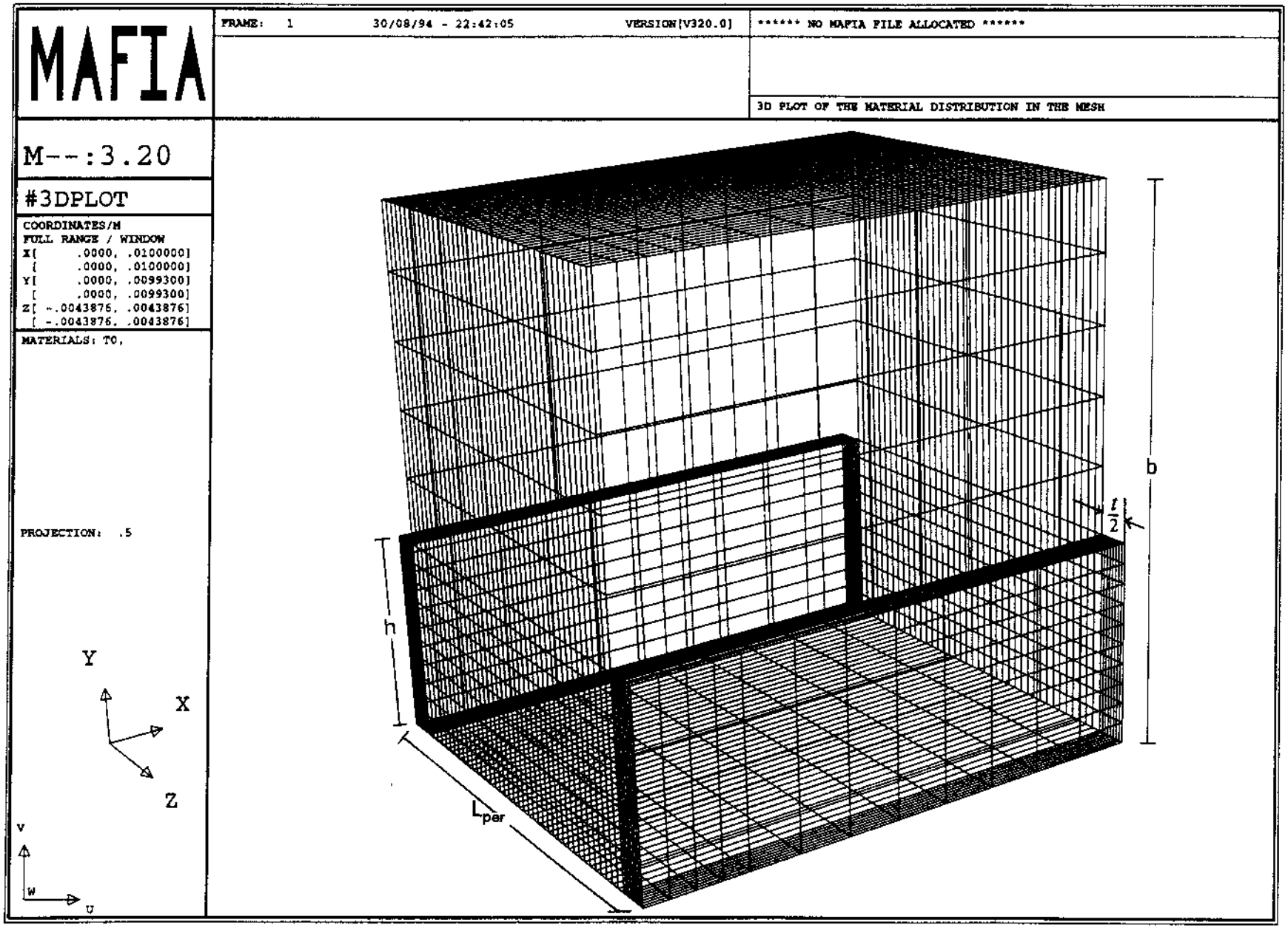

Figure 1 Finite Element Mesh of a Planar Accelerating Cell (1-Quarter Geometry)

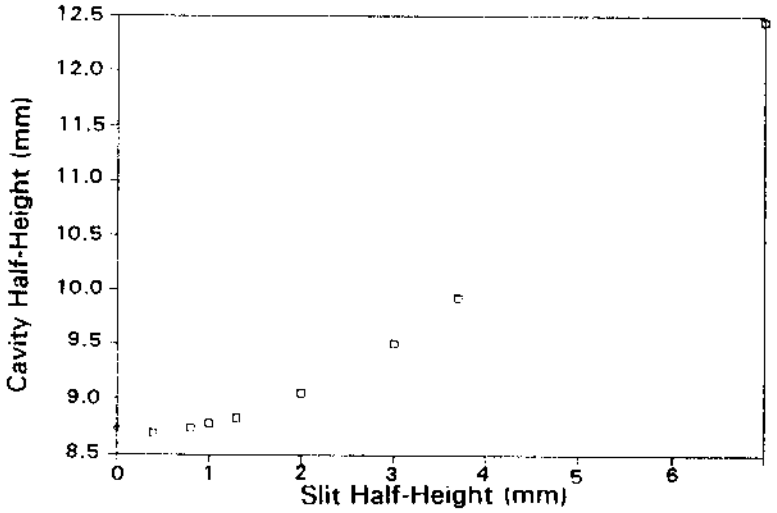

a. Cavity Height vs Slit Height for Fundamental Mode at 11.4 GHz

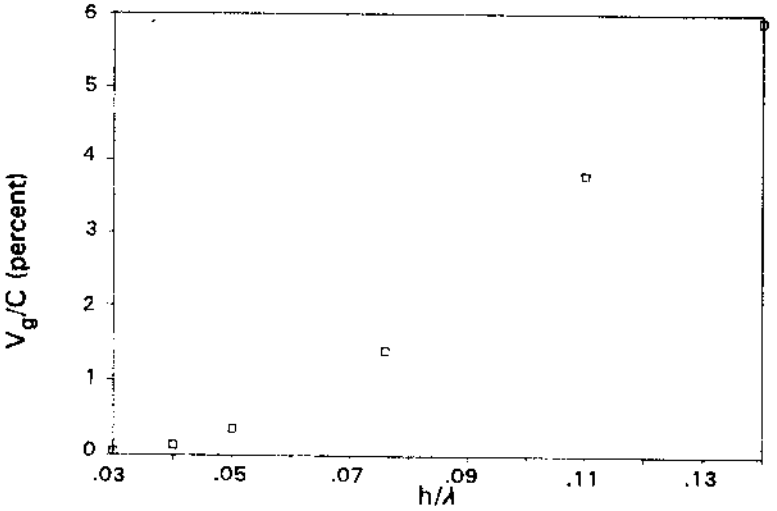

b. Group Velocity vs h/λ

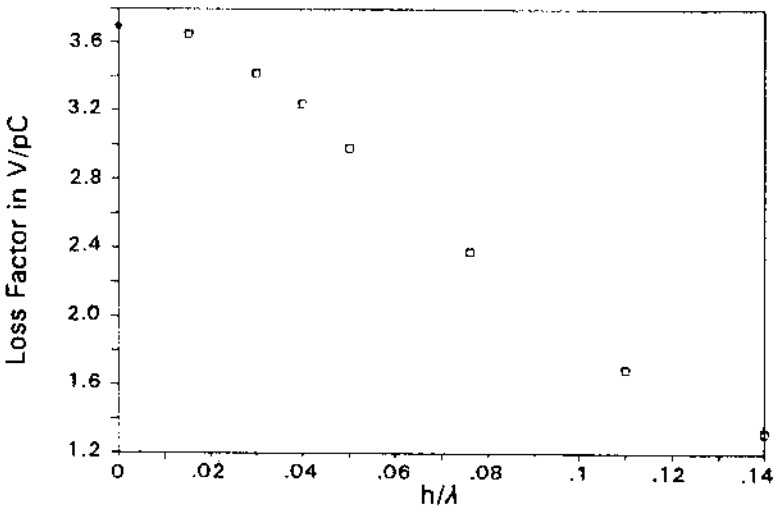

c. Fundamental Mode Loss Factor on Axis vs Slit Height

Figure 2 Properties of Planar Accelerating Structure

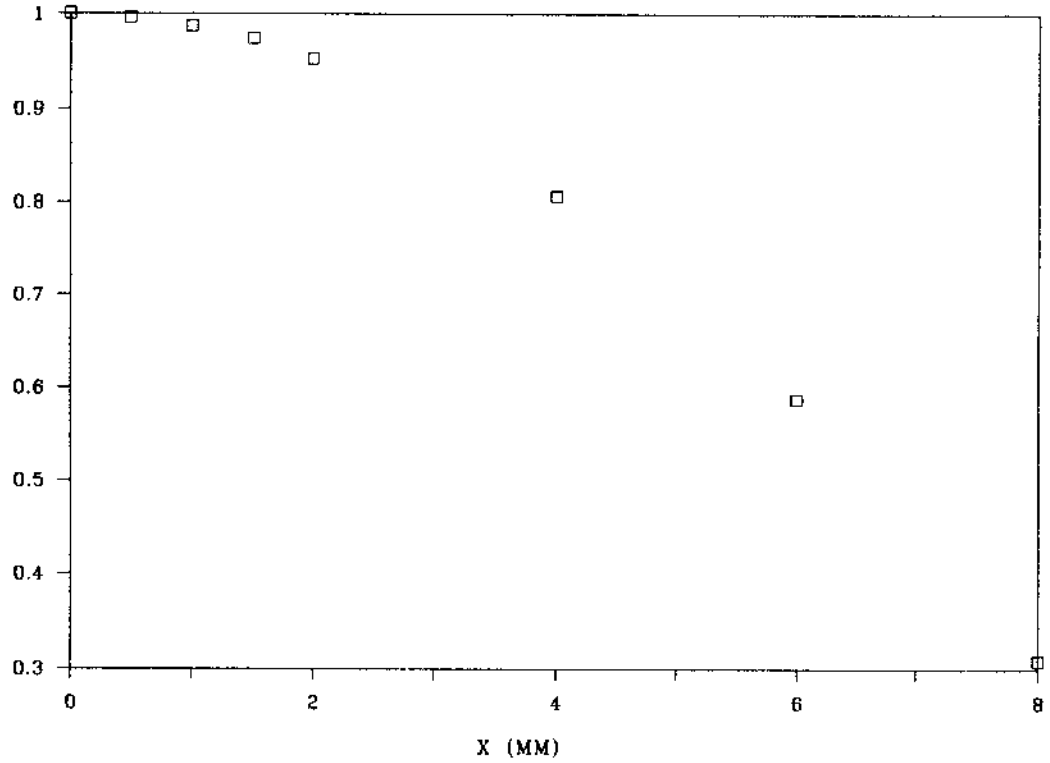

a. Vertical (x)

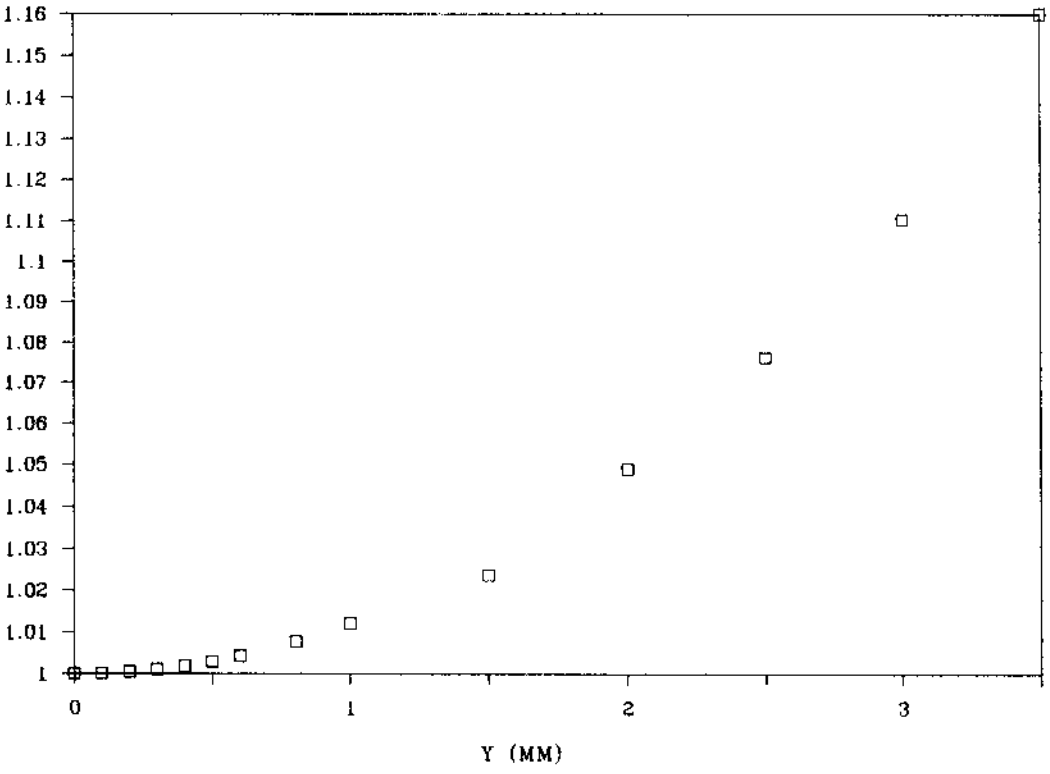

b. Horizontal (y)

Figure 3 Transverse Variations of the Normalized Longitudinal Voltage for PAS, $h/\lambda = .14$

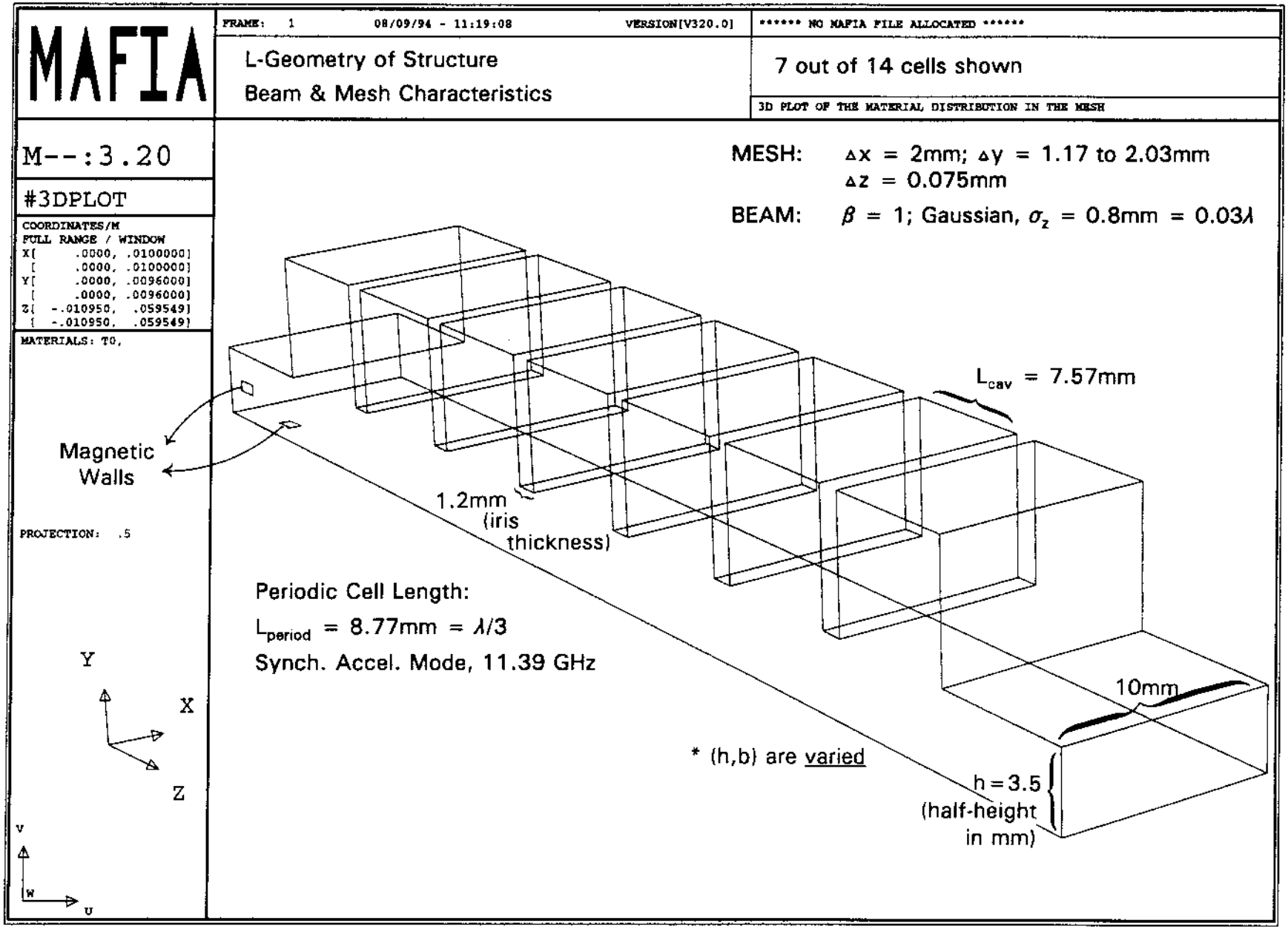

Figure 4 A Planar Accelerating Structure, L-Geometry, 1-Quarter Structure

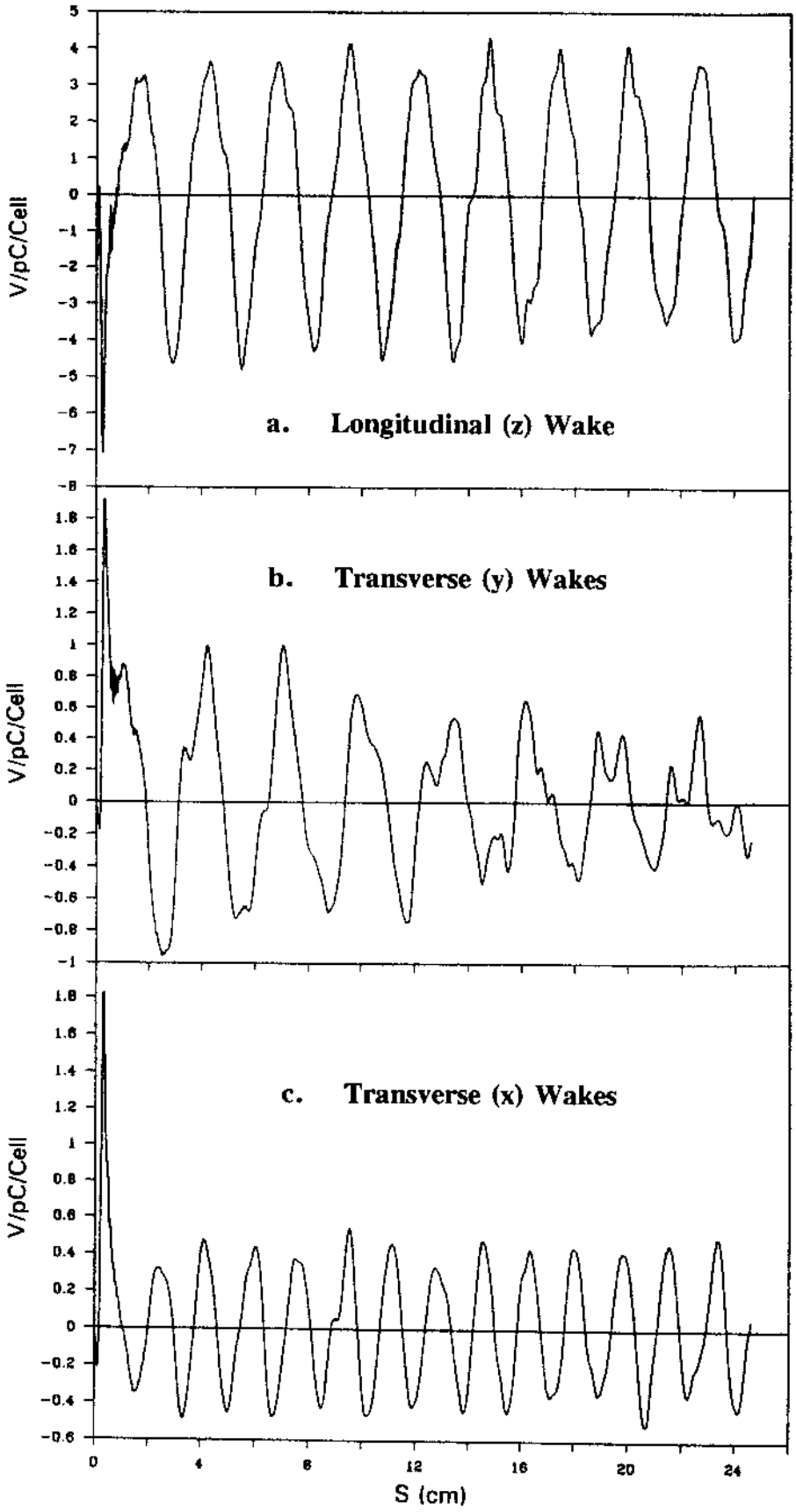

Figure 5 Wake Potential for a 14-Cell PAS